Chemical Engineering Science 258 (2022) 117748

Contents lists available at ScienceDirect

Chemical Engineering Science

journal homepage: www.elsevier.com/locate/ces

Towards best practice recommendations for turbulence modelling of high-pressure homogenizer outlet chambers – Numerical validation using DNS data

Peyman Olad [a,*], Marco Crialesi Esposito [b], Luca Brandt [b], Fredrik Innings [a,c], Andreas Hakansson [a]

[a] Department of Food Technology, Engineering and Nutrition, LTH at Lund University, Lund, Sweden
[b] Flow, Department of Engineering Mechanics, Royal Institute of Technology (KTH), Stockholm, Sweden
[c] Tetra Pak Processing Systems AB, Lund, Sweden

HIGHLIGHTS

- Accurate description of the flow inside emulsification devices is crucial.
- This study compares LES and RANS predictions to DNS validation data for an HPH.
- Both LES and RANS are able to predict the general outline of the flow.
- LES shows slightly better performance than RANS in predicting dissipation rates.
- Low computational cost of RANS keeps it an interesting supplementary tool.

ARTICLE INFO

Article history:
Received 3 February 2022
Received in revised form 2 May 2022
Accepted 15 May 2022
Available online 19 May 2022

Keywords:
High-pressure homogenizer
CFD
Emulsification
LES
RANS
DNS

ABSTRACT

There is a large interest in predicting high-pressure homogenizer (HPH) valve hydrodynamics using CFD, in academic research and industrial R&D. Most of these studies still use two-equation RANS turbulence models, whereas only a few have used LES formulations. From a theoretical perspective, LES is known to be more accurate than RANS, especially in terms of estimating the dissipation rate of turbulent kinetic energy, which is the most important parameter needed for predicting efficiency using a population balance equation (PBE). However, LES also comes at a considerably higher computational cost. To choose the appropriate modelling approach, it is important to understand how much the accuracy and the computational cost increase between RANS and LES.

This study provides the first validation of high-pressure homogenizer hydrodynamics, comparing RANS and a well-resolved LES to numerical experimental validation data of direct numerical simulation (DNS), on a model of the gap outlet jet. The LES does result in a higher accuracy throughout, but the differences are relatively small, when focusing on the flow inside the jet. When using the CFD results to predict maximum surviving drop diameter, the LES results in a relative error of 4.8% whereas the RANS leads to a relative error of 18%. Both errors are substantially smaller than those from a traditional scale-based equation instead of a CFD-PBE. When seen in the substantial reduction of computational time (a factor of 970), results illustrate how RANS could remain a viable supplementary technique for CFD modelling of HPHs, despite its many limitations. Best practice recommendations for obtaining this RANS performance is discussed.

1. Introduction

Being able to accurately describe the flow field inside emulsification devices such as the high-pressure homogenizer (HPH), is of substantial interest, both for the academic emulsification research community and for the chemical engineering industry. One of the principal motivations behind this is the interest in optimizing

Abbreviations: CFD, Computational fluid dynamics; DNS, Direct numerical simulation; DSD, Drop size distribution; FFT, Fast Fourier Transform; HPC, High performance computing; LES, Large eddy simulation; PBE, Population balance equation; PIV, Particle image velocimetry; RANS, Reynolds-averaged Navier-Stokes; TKE, Turbulent kinetic energy; URANS, Unsteady Reynolds-averaged Navier-Stokes.

* Corresponding author.
E-mail address: peyman.olad@food.lth.se (P. Olad).

https://doi.org/10.1016/j.ces.2022.117748
0009-2509/

Nomenclature

D_{32}	Sauter mean diameter, m
D_i	Droplet size in class i
D_{max}	Maximum drop size, m
g_i	Fragmentation rate at size class i
h	Gap height, m.
k	Turbulent Kinetic Energy (TKE), $m^2\ s^{-2}$
$k_{modeled}$	Turbulent Kinetic Energy (TKE) modelled by LES sub-grid model, $m^2\ s^{-2}$
$n_{l,l}$	Fixed pivot redistribution matrix
N_i	Number of droplets in class i
Re	Reynolds number
Re_y	Turbulent Reynolds number
s'_{ij}	Fluctuating rate of strain, s^{-1}
S'	Characteristic filtered rate of strain
t	Time, s.
t_g	Gap time-scale, s
$\|\bar{U}\|$	Time (and spanwise, z) averaged velocity magnitude, m s^{-1}.
U_g	Bulk gap exit velocity, m s^{-1}.
u_x, u_y, u_z	Instantaneous velocity in dimensions x, y, z, m s^{-1}.
u', v', w'	velocity fluctuations in dimensions x, y, z, m s^{-1}.
U_x, U_y, U_z	Time (and spanwise, z) averaged velocity in dimensions x, y, z, m s^{-1}.
x, y, z	Spatial dimensions (see Fig. 1), m.
$y_{1/2}$	Jet half-width, m
y_w	First mesh point wall-distance, m

Greek

ΔP	Homogenizing pressure, Pa
ε	Local dissipation rate of TKE, $m^2\ s^{-3}$.
ε^*	Characteristic dissipation rate of TKE for the device, $m^2\ s^{-3}$.
γ	Surface tension, N/m
μ_C	Dynamic viscosity of the continuous phase, Pa s
μ_D	Dynamic viscosity of the dispersed phase, Pa s
ρ_C	Density of the continuous phase, kg m^{-3}

operation and design of HPHs, to reduce energy consumption and improve the control over the resulting emulsion functionality.

The HPH consists of one or (most typical) two valves connected in series, fed by 3–5 piston pumps. The pumps deliver a high static pressure ($\Delta P \sim 5$–40 MPa) forcing the fluid through the valve consisting of an inlet chamber, where fluid accelerates into a narrow gap (~10–100 μm), reaching high velocities (~100 m/s), and then exiting into a larger outlet chamber (Innings and Trägårdh, 2005). Single drop breakup visualizations show that drop breakup takes place in the turbulent jet created as the fluid exits the gap (Innings and Trägårdh, 2005; Innings et al., 2011; Kelemen et al., 2015; Mutsch et al., 2021).

Experimentally measuring the velocity field inside HPH valves is challenging, partially due to the high static pressures, high velocities and small geometric length-scales, and partially due to the highly confined axisymmetrical geometry of the valve where it has proven difficult to insert probes or get the optical access necessary for experimental investigations. The available experimental studies rely on scaling to reduce velocities and on increasing length-scales and re-designing to allow optical access (see Bisten and Schuchmann (2016) for a comprehensive review). Consequently, computational fluid dynamics (CFD) has long been identified as an important tool for studying HPH valves.

From the 1990s, a large number of such studies have been published: Kleinig and Middelberg (1996) performed the first CFD study on an HPH valve, considering a laminar flow inside the inlet chamber and the gap region of a homogenizer valve. This study predicted pressure gradients for different gap sizes. Later, the same group (Kleinig and Middelberg, 1997), used a Reynolds-Averaged Navier-Stokes (RANS) model (Standard k – ε) to simulate the turbulent flow in the homogenizer outlet chamber. Stevenson and Chen (1997) used CFD to study the relationship between homogenizing pressure and gap height, and were the first to provide detailed information on the velocity and turbulence fields in these devices.

In the 2000 s, the number of studies increased. These studies were mostly based on RANS-based CFD models: Miller et al. (2002) performed a RANS CFD on an HPH valve and compared the performance of different k – ε models, concluding that the realizable k – ε model provides a more accurate estimation of the homogenizing pressure. Floury et al. (2004) carried out RANS CFD on an HPH valve with capability of increasing the pressure up to 350 MPa with a relatively high resolution, resolving the flow close to the wall (low-Reynolds numbers wall treatment). Kelly and Muske (2005) attempted to relate the predicted hydrodynamic forces from a RANS CFD (realizable k – ε) to cell breakage inside an

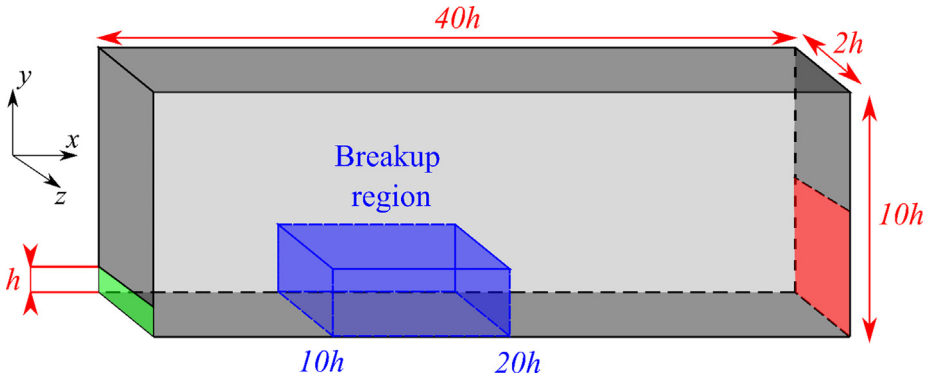

Fig. 1. Schematic view of the HPH outlet chamber model. The green and red planes show the inlet and the outlet boundaries, respectively. The blue box shows the region where breakup is expected to occur. (For interpretation of the references to colour in this figure legend, the reader is referred to the web version of this article.)

HPH. Steiner et al. (2006) used RANS CFD with the standard k – ε model (with low-Reynolds wall treatment) to study the impact of the variation of flow rate and dispersed phase material properties on the drop size distribution (DSD) in the resulting emulsion.

Since the late 2000s, investigators have started to move from using CFD to mainly discuss velocity fields, pressures and turbulence levels, to using the CFD results to model, predict or test emulsification efficiency between designs and operating conditions, either by using Kolmogorov-Hinze theory (Arai et al., 1977; Calabrese et al., 1986; Davies, 1985; Hinze, 1955; Kolmogorov, 1949; Vankova, et al., 2007) or a population balance equation (PBE) formulation (Liao and Lucas, 2009; Ramkrishna, 2000; Solsvik et al., 2013). Köhler et al. (2008) studied a microstructured simultaneous homogenizing and mixing valve using RANS CFD based on RNG k – ε model to investigate the effect of the operating parameters on the predicted fat globules size distribution. Raikar et al. (2010) combined a RANS CFD with a standard k – ε with a PBE to predict the evolution of the DSD in the device. Casoli et al. (2010) used the values of the dissipation rate of the turbulent kinetic energy (TKE) on particle tracks obtained from a RANS CFD with a standard k – ε model for breakup predictions. Håkansson et al. (2013) also connected a PBE to the dissipation rate of TKE on particle tracks through a RANS formulation using a multi-scale k – ε model. Becker et al. (2014) suggested a one-way coupling of PBE and RANS CFD using an RNG k – ε turbulence model, as did Dubbelboer et al. (2014). More recently, Jiang et al. (2019) and Guan et al. (2020) coupled PBE to RANS CFD using realizable k – ε simulations. Pang and Ngaile (2021), with a similar intent, studied three different HPH valve geometries by linking PBE to CFD using realizable k – ε, comparing to experimental data.

As seen from the list above, a large number of studies base their investigations on two-equation RANS CFD models (i.e., k – ε models). CFD simulations on HPH valve using two-equation RANS models are fast, and with the advances of computational power, they are possible to be run on benchtop workstations or even office laptops. However, two-equation RANS turbulence models are also known to have many theoretical limitations, especially when it comes to predicting the dissipation rate of TKE (Pope, 2000) which is the main parameter of interest in the large number of CFD-PBE studies listed above. Experimental validations for these CFD RANS models on HPH valves (or similar geometries) are rare. Håkansson et al. (2012) provided a validation using 2D particle image velocimetry (PIV) data on a scaled HPH valve. These results suggest that the general outline of the outlet chamber jet can be fairly well predicted by using either a realizable k – ε or an RNG k – ε, but that turbulence intensity is misrepresented. However, the most interesting parameter, dissipation rate of TKE, was not available in the study, due to the severe theoretical limitations in using 2D PIV for estimating this quantity (Saarenrinne and Piirto, 2000; Tanaka and Eaton, 2007; Wang et al., 2021).

Aware of the theoretical limitations of RANS CFD, several groups have attempted to move to the theoretically more suitable but more computationally costly large eddy simulations (LES). LES fully resolves the largest turbulent length-scales and models only the smallest ones. Taghinia et al. (2016) used LES and hybrid LES-RANS on the same geometry as Håkansson et al. (2012), thus extending the PIV-validation to include an LES. These authors concluded that the LES model provides a superior performance in terms of predicting the velocity and shear stress fields. More recently, Bagkeris et al. (2020) carried out an LES study on a Sonolator HPH. The authors also included a comparison with experimental PIV data and concluded that the agreement was satisfactory.

As expected from theoretical reasoning on assumptions imposed in LES versus RANS (Pope, 2000), both these studies conclude that LES provides more accurate predictions than RANS. However, the computational cost is also substantially higher. This is an important factor, especially for investigators interested in using PBE to predict emulsification efficiency. The ratio between the number of RANS-based and LES-based studies indicates that the RANS is still the most common modelling strategy for HPH valves. This leads to the question of exactly how large the difference in accuracy between LES and RANS based CFD is for the case of HPH valves.

The generation of high quality validation data (including the dissipation rate of TKE) is of critical importance to answer these questions. Our research group has recently provided a direct numerical simulation (DNS) on a model of a HPH outlet chamber, with careful scaling and geometrical design to capture the main features of the HPH outlet jet (Olad et al., 2022). DNS is often referred to as a numerical experiment since it calculates the turbulent flow properties without modelling assumptions, by fully resolving the flow down to the smallest turbulent structures (at an exceptionally high computational cost). Thus, DNS is a near-ideal source of validation data. DNS is, however, not an alternative to LES and RANS for routinely evaluating industrially relevant devices (due to the computational cost), but it does provide a suitable validation dataset to test and compare the accuracy of LES and RANS on HPH outlet chambers.

The overall aim of this study is therefore to determine how well LES and RANS perform in predicting the flow properties relevant for characterizing the efficiency of the confined turbulent wall jet similar to that in a high-pressure homogenizer, using DNS data for validation. The specific research questions are:

(i) To what extent are the LES and RANS able to reproduce the time-averaged velocity field in the outlet chamber?

(ii) To what extent are the LES and RANS models able to predict the local and characteristic dissipation rate of TKE?

(iii) How large effect will the deviation between true dissipation rate of TKE (DNS data) and the model results (LES and RANS) have on the prediction of the drop diameters in a Kolmogorov-Hinze or PBE framework?

(iv) What are the suitable modelling settings when using a RANS formulation to model the outlet chamber of a HPH?

The rest of the paper is organized as follows: Section 2 introduces the CFD methodology, including a description of the HPH-geometry used in the validation (Section 2.1), the DNS-validation method (Section 2.2), and the two modelling approaches (the LES based CFD in Section 2.3 and the RANS based CFD in Section 2.4). Section 2.5 describes how the turbulent flow-field can be used for a drop-size prediction. Sections 3.1–3.2 compare the modelled flow-fields (LES and RANS) to the validation data. Section 3.3 compares the predicted dissipation rates of TKE between models and validation data, and investigates what this implies in terms of a difference in predicted emulsion drop size. Section 3.4 examines the differences between the RANS models whereas Section 3.5 compares the CFD-methods in terms of computational cost and Section 3.6 discusses best practices for HPH valve CFD. Finally, a summary of the main findings is presented in Section 4.

2. Methodology

2.1. HPH geometry

The validation is performed on a simplified HPH outlet chamber geometry, illustrated in Fig. 1. The motivation for using this model (instead of the HPH outlet chamber in the typical production scale device) is to capture as many critical elements as possible of the HPH outlet chamber flow (jet-flow, wall-adherence, confinement),

in a cuboidal domain of limited size (a requirement for enabling DNS). A comprehensive discussion of the scaling and how the geometry and fluid properties are chosen to describe the flow in an HPH outlet can be found elsewhere (Olad et al., 2022). In brief, the most important dimensionless numbers (Reynolds number, gap height to Kolmogorov micro-scale ratio, and boundary layer thickness to Kolmogorov micro-scale ratio) are set to be in the range of those of a production- and a pilot-scale homogenizer.

Fig. 1 shows the dimensions of the computational geometry, in units of gap heights, h, where h = 750 μm. The red and green faces represent the outlet and inlet of the domain. The blue box indicates the region where breakup of droplets is expected to take place, as suggested by previous studies (Innings et al., 2005; Innings et al., 2011). The dark grey facets denote the walls. With a bulk inlet velocity of U_g = 16 m/s, this setup corresponds to a Reynolds number Re = 2057 when assuming a fluid density ρ_C = 1200 kg/m^3 and viscosity μ_C = 7.0 mPa s. Moreover, the problem is studied as isothermal.

2.2. Validation data (DNS)

DNS-calculated velocity fields are used as the validation data in this study. A comprehensive discussion on the DNS methodology and the resulting turbulent flow statistics is available elsewhere (Olad et al., 2022). In brief, an in-house DNS code, validated in several previous studies (Picano et al., 2015; Rosti and Brandt, 2017; Rosti et al., 2019), is used. The code uses an FFT solver for the pressure Poisson equation. Second-order central differencing and Adam-Bashforth schemes are used for the spatial derivatives and time-stepping, respectively. A total of 173 million grid points are used in a Cartesian grid. The inlet boundary condition is imposed using the method suggested by Billson et al. (2003) and Davidson and Billson (2006), where anisotropic synthetic velocity fluctuations are generated and added to a scaled average velocity profile obtained from a PIV investigation on a similar geometry (Håkansson et al., 2011), scaled to account for the difference in Reynolds number (Olad et al., 2022). The outlet boundary condition follows the suggestion by Orlanski (1976). A 2 h thick slice (spanwise, z-direction, see Fig. 1) of the geometry is simulated, using periodic boundary conditions, to reduce computational cost (Olad et al., 2022).

The DNS is initiated from a zero velocity field and iterated until converged, after ~ 2000 t_g, where $t_g = h/U_g$ (=47 μs), is a representative gap time-scale. The time-averaged velocities and dissipation rates of TKE used here are averaged across a sampling interval of 3000 t_g.

2.3. LES modelling methodology

The LES is set up in a commercial software (Fluent 19.0, Ansys, Canonsburg, PA) using a Dynamic Smagorinsky-Lilly formulation (Germano et al., 1991; Lilly, 1992) as subgrid scale model for the turbulence. The SIMPLEC algorithm is used for the coupling of velocity–pressure fields with second order and bounded central differencing schemes for the discretization of the pressure and momentum terms, respectively. A simple three-level second order implicit scheme is used for time stepping. The mesh is structured and stretched and the mesh size is in the range (0.004 h, 0.28 h) in the wall-normal direction y, (0.055 h, 0.33 h) in the streamwise direction x, and constant size of 0.051 h in the spanwise direction z. In terms of wall resolution, the LES mesh gives a y^+ in the range (0.5, 2.5) on the lower wall.

The same experimental velocity profile was prescribed at the inlet boundary as for the DNS. As in the DNS, this needs to be supplemented by an inlet-boundary condition turbulence model, and several alternatives are available. In this study, the vortex method (ANSYS, 2019; Mathey et al., 2006) is used to generate the turbulence at the inlet boundary; random 2D vortices are added to the mean velocity profile in the plane normal to the inlet, locally adjusted to estimate the velocity fluctuations based on the local levels of TKE (Mathey et al., 2006). Preliminary studies of the DNS showed that the turbulence at the inlet does not substantially affect the turbulence at the active region of breakup (shear layer of the jet), due to the fact that the flow at the inlet (i.e. HPH valve gap exit) is in a transient regime and the turbulence intensity is lower than that in the jet shear layer. Consequently, we do not expect any significant difference in the flow behavior by changing the synthetic turbulence generation method at the inlet.

The average velocities (required as inputs by the vortex method) are obtained from a PIV study on a similar system (Håkansson et al., 2011). The dissipation rate of TKE and the Reynolds-stress components on the inlet boundary are taken from the DNS (Olad et al., 2022). The outlet is modelled as a constant pressure outlet (zero static gauge pressure). No-slip boundary conditions are imposed on all walls. As with the DNS, a 2 h spanwise slice is modelled, using periodic boundary conditions.

A stretched mesh with approximately 1.85 million grid points is used. This implies that almost 95% of the total TKE is resolved throughout the domain (See Fig. 2), with some exceptions close to the inlet, where the percentage of the resolved TKE,

$$k = \frac{1}{2}(u'u' + v'v' + w'w') \tag{1}$$

is about 80–90%. The resolution, thus, satisfies the minimum requirement of at least 80% of total TKE resolved as suggested in the literature (Pope, 2000).

The LES is first run until convergence, and then for 13 000 t_g to collect statistics. To verify that the flow is truly converged before starting to sample, a methodology similar to that for the DNS is used (Olad, Crialesi, Brandt, Innings, & Håkansson, 2022): the running average of the streamwise velocity component is studied as a function of the simulation time, at different points in the domain (using a window size of 0.2 s = 4 300 t_g), see Fig. 3. The dashed horizontal lines indicate the 5% margin below and above the final averaged value for the lines of same color. For all three positions in Fig. 3 (chosen in the regions where drop breakup is expected), the simulation is converged after 4000 t_g. The choice of basing this analysis on velocity was due to the observation that the large recirculation eddy above the jet is the slowest, and consequently, the limiting factor for convergence (Olad et al., 2022).

In the LES model, the dissipation rate of TKE is calculated as follows:

$$\varepsilon = 2(\nu_t + \nu)\langle S'^2 \rangle \tag{2}$$

where S' is the characteristic filtered rate of strain, defined as:

$$S' \equiv (2s'_{ij}s'_{ij})^{1/2} \tag{3}$$

and s'_{ij} is the fluctuating rate of strain:

$$s'_{ij} = \frac{1}{2}\left(\frac{\partial u'_i}{\partial x_j} + \frac{\partial u'_j}{\partial x_i}\right) \tag{4}$$

where ν_t is the turbulent viscosity, and ν is the molecular kinematic viscosity.

2.4. RANS modelling methodology

The 2D steady RANS model is set up in the same commercial CFD software (Fluent 19.0, Ansys, Canonsburg, PA), using a two-equation RNG k – ε turbulence model (Yakhot and Orszag, 1986). Similar to the LES, the RANS mesh is also structured and stretched and the mesh size is in the range (0.0017 h, 0.2192 h) in the wall-

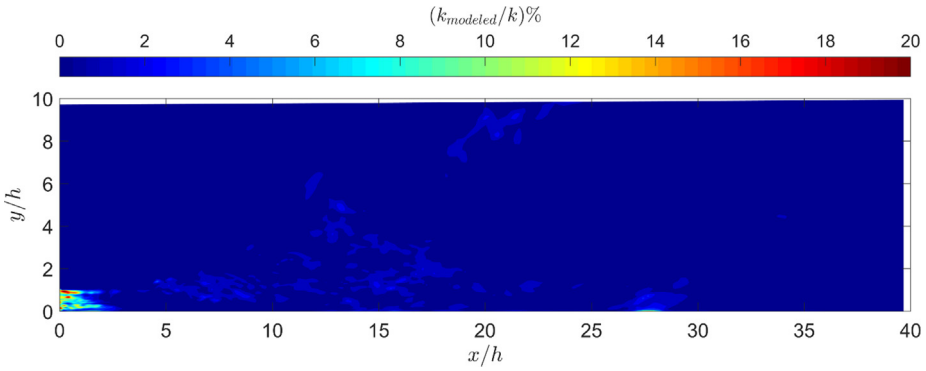

Fig. 2. Percentage of modelled turbulent kinetic energy (TKE) in the LES formulation.

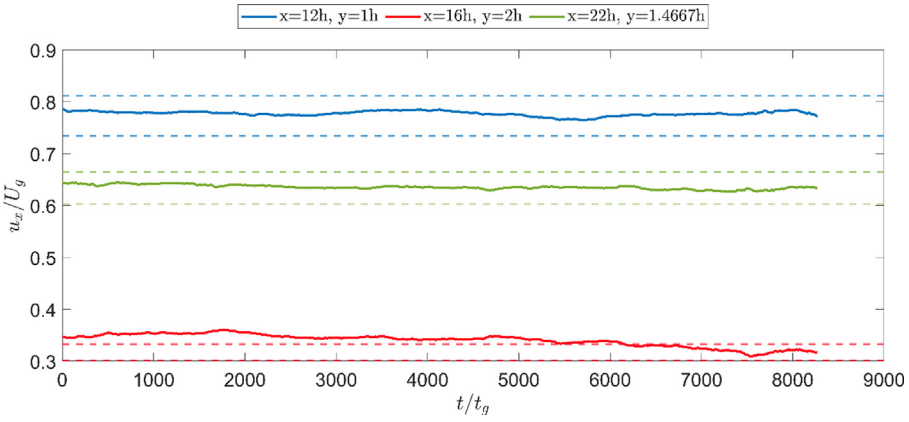

Fig. 3. Running average of streamwise velocity, u_x, at different points in the spanwise plane (z/h = 1) with window size of 0.2 s (4300 t_g). The horizontal axis shows the normalized time from the beginning of the simulation.

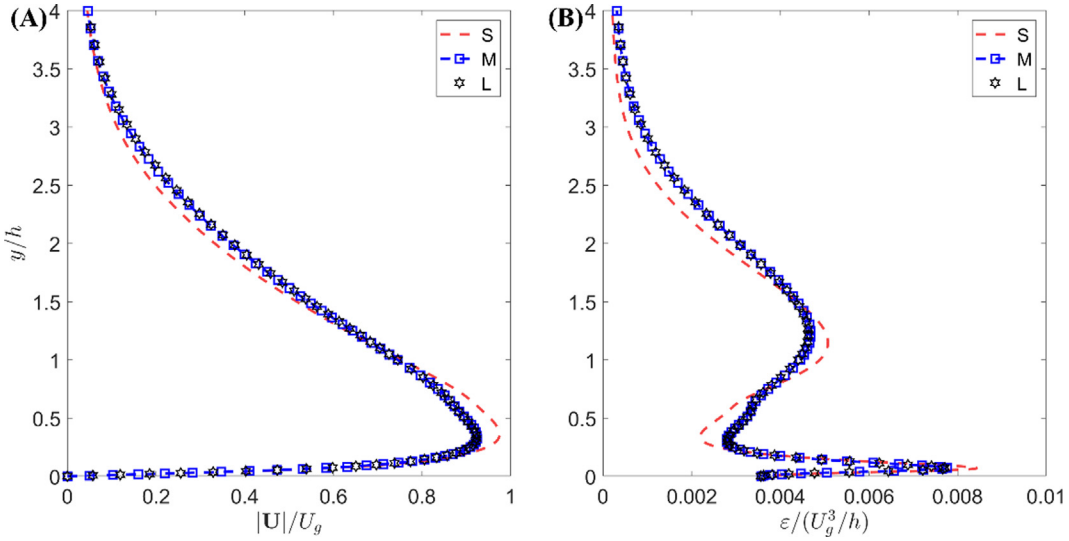

Fig. 4. Investigating the mesh independence across RANS meshes. (A) velocity magnitude, |U|, as a function of wall-normal distance, y. (B) dissipation rate of TKE, ε, as a function of wall normal distance, y. (x/h = 16).

normal direction y, (0.03 h, 0.35 h) in the streamwise direction x. In terms of wall resolution, the RANS mesh gives a $y^+ < 0.5$ everywhere on the lower wall.

The enhanced wall-treatment option in Fluent was used. This means that local near-wall mesh resolution determines the treatment of the flow close to the wall i.e. if the near-wall mesh is sufficiently fine (if the first point is located at $y^+ < 0.5$), a so-called 'two-layer model' is used. In this model, the wall region is divided into the viscosity-affected and fully-turbulent regions based on the turbulent Reynolds number defined as:

$$\mathrm{Re}_y \equiv \frac{\rho_C y_w \sqrt{k}}{\mu_C} \tag{5}$$

where y_w is the first mesh point wall distance. If, $\mathrm{Re}_y > 200$, the turbulence model is used (RNG k – ε). In the viscosity affected region, the one-equation model of Wolfshtein (1969) is used i.e. the equation of TKE and momentum are the same as those of the turbulence model, but the turbulent viscosity is defined differently. If the mesh resolution is insufficient close to the wall, the modified law of the wall suggested by Kader (1981) is used in which a blending function enables a single expression for the logarithmic and laminar formulations of the law of the wall. (Due to the high resolution of the mesh close to the wall in the RANS simulation of the present study i.e. first point located at $y^+ < 0.5$, no wall functions are activated.).

The SIMPLE algorithm is used for the coupling of the velocity–pressure fields and second order discretization is used for all terms. On the inlet boundary, the (scaled) velocity and TKE profiles from the PIV study (Håkansson et al., 2011) are imposed. The outlet is modelled as a constant pressure outlet (zero static gauge pressure). No-slip boundary conditions are imposed on all walls.

To verify that the results of the RANS study are independent of the numerical resolution, three meshes with different densities are created: mesh S (45,000 cells), mesh M (85,000 cells) and mesh L (128,000 cells). Fig. 4 shows the profiles of the normalized velocity magnitude and dissipation rate of TKE, at a streamwise location of x/h = 16, comparing the three different mesh densities. As seen in the figure, increasing the number of computational cells from 85,000 (M) to 128,000 (L) does not further improve the results. All subsequent RANS simulations are, therefore, run with mesh M.

Moreover, an unsteady RANS (URANS) (using three-level second order implicit time-stepping) is performed to investigate if any improvements could be obtained by allowing for a transient formulation (see Sections 3.4.1). To investigate the effect of the specific two-equation turbulence model used, three additional steady-state CFD models are compared: standard k – ε (Launder and Spalding, 1972), realizable k – ε (Shih et al., 1995) and SST k – ω (Menter, 1994) (see Section 3.4.2).

2.5. Emulsion drop size predictions

From an applied perspective, knowing the relative error obtained in predicting the jet velocity or dissipation rate of TKE, is less interesting (and more difficult to interpret). It is more relevant to quantify what such a difference corresponds to in terms of errors in the prediction of the drop diameters produced by the devices. As discussed in the introduction, estimating dissipation rates of TKE (or time-histories thereof) is typically the main objective of CFD investigations of these devices in most recent studies.

The maximum drop diameter resulting from prolonged exposure of an emulsion to a turbulent field characterized by a dissipation rate of ε* can be accurately predicted by the drop-viscosity corrected Kolmogorov-Hinze theory (Arai et al., 1977; Calabrese et al., 1986; Davies, 1985; Hinze, 1955; Kolmogorov, 1949; Vankova et al., 2007). When the resulting drop diameter is larger than the Kolmogorov length-scale, the relationship is:

$$D_{\max} = 0.86\left(1 + 0.37\frac{\mu_D \varepsilon^{*1/3} {D_{\max}}^{1/3}}{\gamma}\right)\varepsilon^{*-2/5}\gamma^{3/5}\rho_C^{-3/5} \tag{6}$$

Note that Kolmogorov-Hinze theory describes the effect of turbulence on breakup in terms of a single 'characteristic dissipation rate of TKE', ε*, whereas the turbulent field is spatially inhomogeneous in an emulsification device. The characteristic dissipation rate of TKE is typically interpreted as the average value in the effective region of breakup. In this study it is defined as the value averaged across the early jet region, 0 < x/h < 20, 0.5 < y/h < 2.5.

The maximum surviving drop diameter as predicted by the validation data (DNS) was compared to that obtained using the two turbulence models using Eq. (6): The characteristic dissipation rate of TKE from the DNS is used to calculate the validation 'true' D_{max}. This is compared to the dissipation rates of TKE averaged across the same region from the LES and the RANS. The characteristic dissipation rate of TKE is also calculated using two well-known simple empirical expressions (Mohr, 1987),

$$\varepsilon^* = \frac{U_g^3}{20h} \tag{7}$$

and (Innings and Trägårdh, 2007),

$$\varepsilon^* = \frac{U_g^3}{80h} \tag{8}$$

Eqs. (7) and (8) (or a similar expression) would be what typically is used as the input to Eq. (6) in a study not using CFD to describe the device hydrodynamics (cf. Håkansson, et al., 2009; Maindarkar, et al., 2015). All comparisons were made under the conditions ensuring scale similarity between the simplified geometry (Fig. 1) and the industrially relevant HPHs (μ_D = 35 mPas, γ = 20 mN/m, ρ_C = 1200 kg/m^3, see discussion in Section 2.2 and by Olad et al. (2022)).

Alternatively, the evolution of the entire drop size distribution (DSD) can be described using a PBE. Assuming no coalescence, the PBE is discretized into (Kumar and Ramkrishna, 1996),

$$\frac{dN_i}{dt} = -g_i \cdot N_i + \sum_{l=i}^{I} n_{l,i} \cdot g_l \cdot N_l, \tag{9}$$

where N_i is the number of drops in class i, $n_{l,i}$ is the fixed pivot redistribution matrix (Kumar and Ramkrishna, 1996) and g_i is the fragmentation rate evaluated at size class i. A large number of fragmentation rate and fragment size distribution functions have been suggested in previous studies, and comprehensive reviews are available elsewhere (Liao and Lucas, 2009; Solsvik et al., 2013). In this contribution, the free fragmentation rate parameter suggested by Luo and Svendsen (1996) is used together with the assumption of binary breakup with a uniform fragment size distribution. A geometric discretization with I = 50 size classes is used. The resulting 50 ordinary differential equations are solved with a variable order differential equation solver, implemented in ode15s in MATLAB (MathWorks, Natick, MA). A non-negativity constraint is used on all size classes.

To provide a meaningful comparison of how accurate the LES and RANS models would be if used in a PBE setting, the discretized PBE i.e. Eq. (9) is solved at the centerline of the jet. The solution of the DNS is taken as the 'true' value, and compared to the results obtained when using the LES and RANS models.

The surface-averaged drop diameter at the exit, D_{32}, is used as a characteristic average of the DSD:

$$D_{32} = \frac{\sum N_i \cdot D_i^3}{\sum N_i \cdot D_i^2} \tag{10}$$

3. Results and discussion

3.1. Predicting the overall flow outline

The first research question is to what extent the RANS and LES modelling strategies are able to predict the general outline of the HPH outlet chamber flow. Fig. 5A presents contours of the mean velocity magnitude, with red vectors representing the local flow directions in the xy-plane, from the DNS validation data. The thick black lines show the walls of the domain. The flow enters the con-

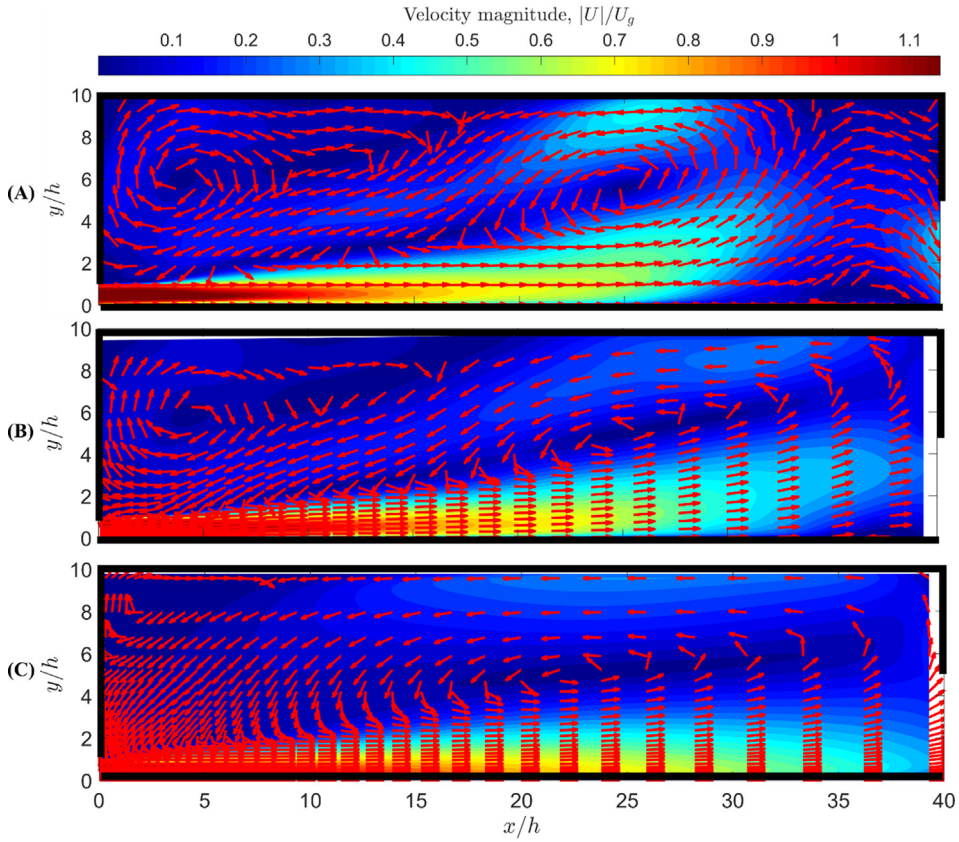

Fig. 5. Velocity magnitude comparing the validation data (A) (Olad et al., 2022) to the turbulence models: (B) LES and (C) RANS. Arrows (red) denote average velocity vectors. (For interpretation of the references to colour in this figure legend, the reader is referred to the web version of this article.)

fined domain from the gap exit, located at the bottom-left of the domain, creating a turbulent wall-jet with macroscopic recirculating vortices above it. This general behaviour is captured by both the LES (Fig. 5B) and the RANS (Fig. 5C).

However, some differences can be seen when investigating the details of the larger vortices. The validation results from the DNS study (Fig. 5A) show two main vortex structures in the outlet chamber. One vortex (the 'outlet vortex') is observed at the approximate position of x/h = 25, y/h = 5.5. This vortex is induced by the presence of the upper wall. Another vortex (the 'inlet-vortex') is observed just above the jet inlet at position x/h = 4, y/h = 6. Both these vortices are a consequence of the confinement of the outlet chamber jet, chosen by design to capture the properties of the outlet chamber of a production scale HPH valve. It is the backflow above the jet body which leads to the generation of the outlet vortex, which forces the jet towards the lower wall and decreases the spreading rate of the jet compared to an unconfined jet (Olad et al., 2022), as observed for the HPH outlet chamber in previous investigations (Innings and Trägårdh, 2007).

Fig. 5B presents the flow solution of the LES model. Some differences can be observed: The same two macroscopic vortices can be seen but with minor differences in position. A slightly more uniform velocity profile can also be seen at the outlet boundary compared to the DNS (most likely due to the difference in outlet boundary condition specification, as discussed in Sections 2.2-3). This implies that the LES model is somewhat misrepresenting the flow close to the outlet. However, for the main part of the jet, especially in the region where breakup is expected (see Fig. 1), the general flow outline predicted with the LES is very similar to the validation data.

Fig. 5C displays the data from the RANS model. It, too, is able to predict the presence of the inlet vortex, but with a significant shift towards the upper wall. The outlet vortex is predicted almost at the same position as that obtained from the LES (at a slight offset from the validation data). Furthermore, the RANS model fails to predict the interaction region between the two vortex structures seen in the DNS validation data.

For a more detailed comparison into the performance of the two turbulence modelling strategies for predicting the time-averaged velocity field, Fig. 6 illustrates the streamwise velocity profiles at four positions downstream the gap exit (x/h = 8, 12, 16, and 22). Starting with the first position (x/h = 8), the validation data clearly show the presence of the inlet vortex, with a region of negative velocities in 2 < y/h < 7. This recirculation zone is still present further downstream of the gap (x/h = 12, 16 and 22), but positioned further out from the lower wall. As seen in Fig. 6, the LES model is able to almost perfectly capture this behaviour up to and including x/h = 16. At the last position, however, the LES underestimates the recirculation vortex. Again, this illustrates that the LES captures the inlet vortex well, but struggles with the outlet vortex (where the outlet boundary condition starts to influence the flow field). The RANS model misrepresents both vortices which can also be seen in the underestimation of the recirculation zone at all profile locations (Fig. 6).

The main jet is, however, of special interest since it is here that the most drop breakup events are expected to take place. Confining the analysis to this region (0 < y/h < 2), the RANS performs substantially better. In this region, there is no substantial improvement in accuracy in the LES as compared to the RANS.

In summary, both modelling approaches capture the overall behaviour. As expected, the LES performs better than the RANS in predicting the interacting macroscopic vortices acting on the jet. Both models perform well in the region where breakup is expected. Here it could also be mentioned that it is the severe confinement

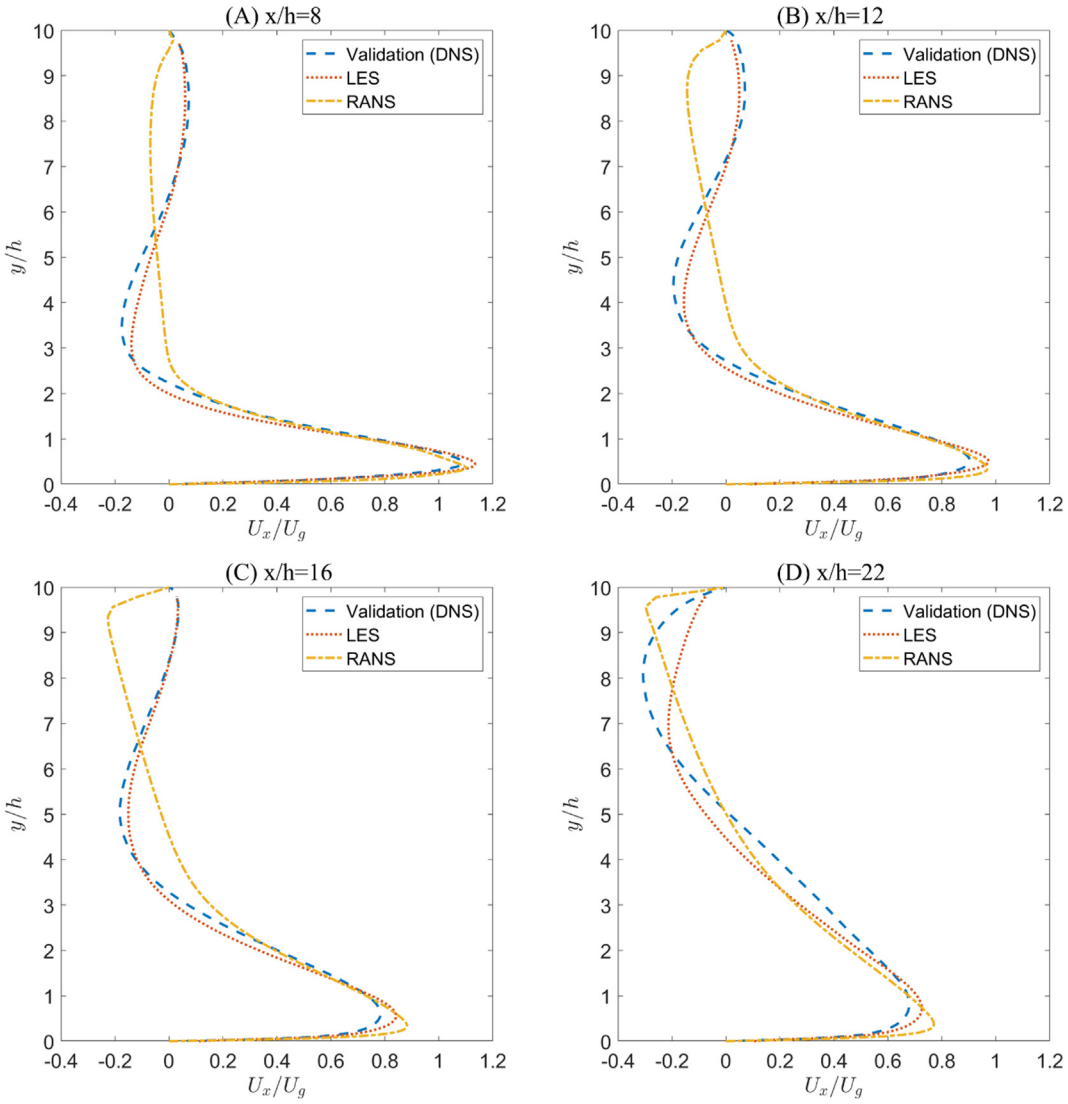

Fig. 6. Average streamwise velocity, U_x, as a function of wallnormal distance, y, comparing the two turbulence models (LES and RANS) to the validation data (DNS). (A) x/h = 8. (B) x/h = 12. (C) x/h = 16. (D) x/h = 22.

that appears to be especially challenging for the models (in particular, the RANS), and that these confinement effects are smaller in the production scale HPH valve than in the model used here. Thus, the RANS and LES may be expected to perform at least as well if applied to an industrially used HPH valve.

3.2. Predicting the jet half-width and centerline velocity

The extent and properties of the outlet chamber jet are of special interest because it is where the breakup is expected to take place. To further investigate how well this is described by the modelling approaches, Fig. 7 compares the jet half-width and centerline velocity. Fig. 7A displays the jet half-width, $y_{1/2}$ – i.e., the position where $U_x(y) = 0.5\ U_{x,max}$, a measure for the jet half-width, as a function of the streamwise position, and Fig. 7B displays the normalized jet maximum velocity, $U_{x,max}/U_g$, as a function of the streamwise position. The validation data show a widening jet (increasing $y_{1/2}$) with distance, and a decreasing jet velocity. A notable shift, with an increased half-width and increased velocity decay rate, can be seen at $x/h \sim 22$, due to the action of the outlet vortex (see discussion in Olad et al., 2022). When comparing this to the turbulence modelling approaches, the results show that both the LES and the RANS underpredict the spreading rate and overpredict the centerline velocity almost everywhere, i.e. they underpredict the deceleration of the jet. This can be contrasted with reports on RANS in non-confined jets (Gerodimos and So, 1997) where an overprediction of the jet spreading rate is observed. This difference is due to the failure of RANS model to correctly predict the interaction of the vortex above the jet and consequently, pushing it towards the wall.

The LES model provides a better estimate (in general closer to the validation data), especially upstream of $x/h \approx 22$ where the confinement and outlet boundary starts to influence the flow substantially. Nevertheless, the differences are relatively small, especially where breakup is expected to take place. Looking at x/h = 12, as example, the relative error in jet centerline velocity is 6.9% with the RANS and 7.5% with the LES. The relative error for the jet half-width is −7.8% with RANS and −13% with LES.

In summary, both LES and RANS are able to describe the development of the main jet with relatively high accuracy and the differences between the two are relatively small.

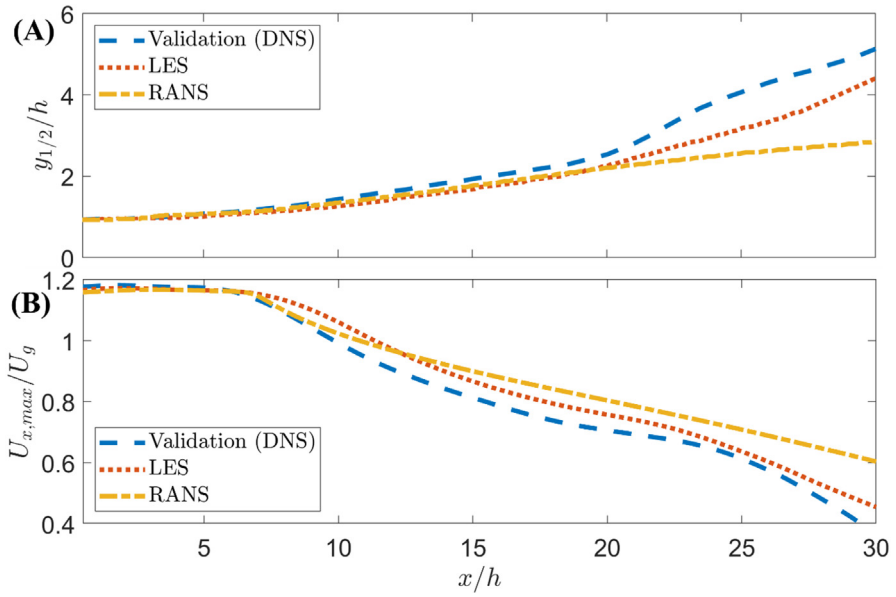

Fig. 7. (A) Jet half-width ($y_{1/2}$) as a function of streamwise position, x. (B) Maximum streamwise velocity along the jet centerline of the jet. $U_{x,max}$, as a function of streamwise position. Comparing the validation data (DNS) to the two turbulence models (LES and RANS).

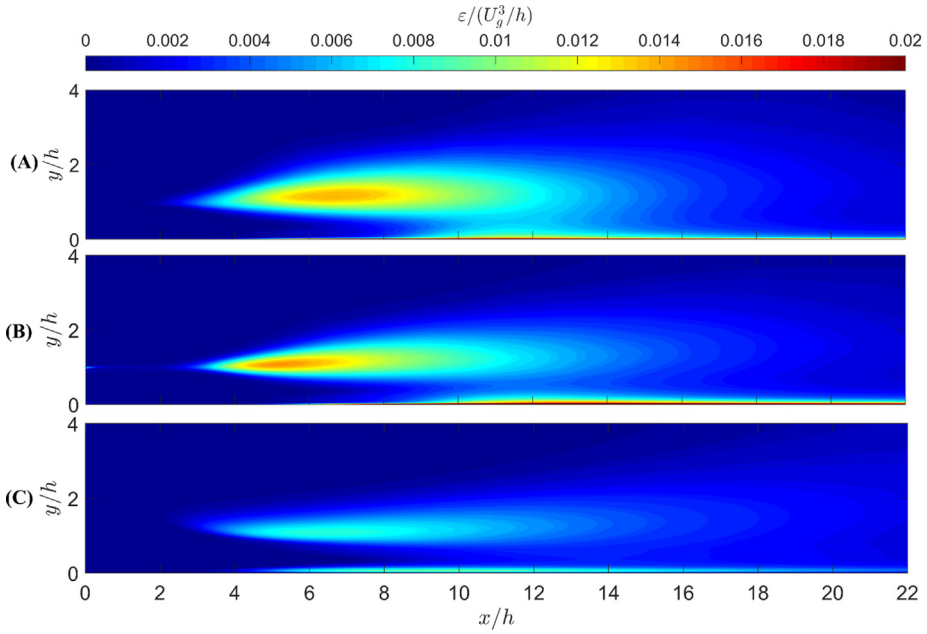

Fig. 8. Dissipation rate of TKE, ε, comparing validation data (DNS) (A) with the predictions obtained with the turbulence models: (B) LES and C) RANS.

3.3. Predicting the dissipation rate of TKE

As mentioned in the introduction, most investigators suggest drop breakup in HPH valves to be caused mainly by turbulent interactions, and that the stress on the drop (or the rate of drop breakup) can be predicted using the dissipation rate of TKE (Arai et al., 1977; Calabrese et al., 1986; Davies, 1985; Hinze, 1955; Kolmogorov, 1949; Vankova et al., 2007). At the same time, dissipation rate of TKE is generally understood as difficult to estimate, especially using two-equation RANS modelling approaches (Pope, 2000). The second research question we address here is, therefore, how close the RANS and LES models are to the validation data in terms of this important parameter.

3.3.1. Overall agreement with validation data

Fig. 8 illustrates the contours of normalized dissipation rates of TKE. The validation data (DNS, Fig. 8) shows the large dissipation region inside the shear layer at x/h ≈ 4–12, as expected for a turbulent jet. A narrow region of high dissipation rate of TKE can also be found close to the lower wall. Note the initial confinement of high dissipation rates of TKE to the shear layers. Thus, a fluid element travelling through the center of the jet will not experience high dissipation rates of TKE before reaching approximately x/h = 10, where the dissipation from both upper and lower shear layer has spread and reached the jet center.

Fig. 8B–C show the predictions using the LES and RANS models. Both the LES and the RANS models under predict the width of the

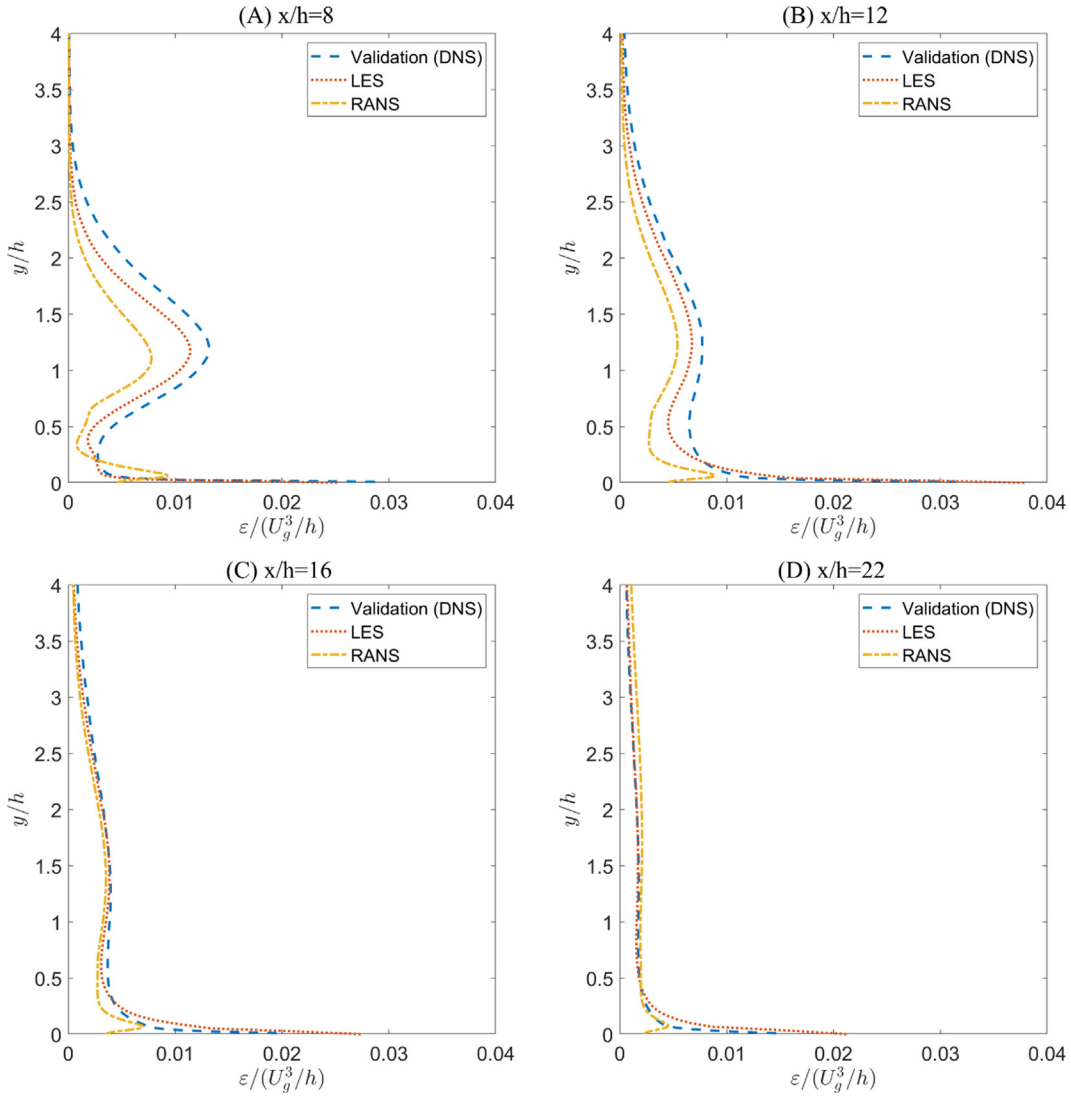

Fig. 9. Dissipation rate of TKE, ε, as a function of the wallnormal distance, y, for the two turbulence models (LES and RANS) and the validation data (DNS). (A) profiles at x/h = 8. (B) x/h = 12. (C) x/h = 16. (D) x/h = 22.

high dissipation rate of TKE. The LES model captures the maximum value relatively well (the relative error is +4% for the global maximum when disregarding the thin inner shear layer) whereas the RANS underpredicts the global maximum by 41%.

A more detailed comparison on the ability of the CFD models to predict the dissipation rate of TKE can be seen in Fig. 9, where we display the wall-normal profiles of the dissipation rate of TKE at four streamwise positions, focusing on the region where breakup is expected to occur (For a similar comparison of the TKE profiles, see the supplementary material). The validation data show that the dissipation rate of TKE profile displays two clearly distinguished peaks located in the inner and outer shear layers of the jet at the first position (x/h = 8). Moving further downstream (x/h = 12–16), these shear layers merge, creating a lower but more uniform level throughout the jet. Note that the validation data show that the highest local dissipation rates of TKE are found in a thin layer close to the wall. This region is, however, of less interest from an applied emulsification perspective, since velocities are low, and, thus, very few drops interact with the continuous phase flow at these positions.

The two-equation RANS models are known to struggle with phenomena such as laminar–turbulent transition, separation, reattachment and boundary layer growth (Pope, 2000), of which the latter two are present in the case of this study. A previous study using PIV data to validate RANS CFD for HPH-valves (Håkansson et al., 2012), argued that part of the inability of the two-equation RANS models to predict all aspects of the flow was due to that the models over-predicted the production of TKE in most of the domain. Hence, they failed to capture positions of negative production (due to the inherent formulation of production of TKE in a two-equation RANS model). This problem is expected when having curved streamlines, which we have due to the presence of strong vortices above the jet.

Summarizing the findings in this section, the LES does improve the accuracy, but provided the substantial simplifications used in a two-equation RANS turbulence model (as compared to a highly resolved LES), the RANS agreement is surprisingly good.

3.3.2. Average dissipation rate of TKE

From an applied emulsification perspective, dissipation rates of TKE (whether estimated from a scaling average or from CFD calculations) are primarily used for assessing the efficiency of the device, i.e., to predict the largest drop diameter surviving a passage (via a Kolmogorov-Hinze type of approach) or to predict the result-

Table 1
Average dissipation rate of TKE and drop diameter predictions. Comparing validation data (DNS), to the CFD turbulence models (LES and RANS) and to traditional scaling estimations suggested in previous studies (Eqs. (7)–(8)).

		Characteristic dissipation rate of TKE		Maximum drop diameter*		Sauter mean diameter	
		ε^* [m^2/s^3]	Relative error [%]	D_{max} [μm]	Relative error [%]	D_{32} [μm]	Relative error [%]
Validation data (DNS)		$2.4{\cdot}10^4$		27.0		20.7	
LES		$2.1{\cdot}10^4$	−12%	28.3	+4.8%	25.6	+24%
RANS		$1.5{\cdot}10^4$	−38%	31.9	+18%	25.2	+22%
Scale-based estimations	Eq. (8)	$6.8{\cdot}10^4$	+190%	18.9	−31%	9.6	−54%
	Eq. (7)	$27{\cdot}10^4$	+730%	11.7	− 57%	4.7	−77%

* Obtained using Eq. (6) on the estimates in the left column.

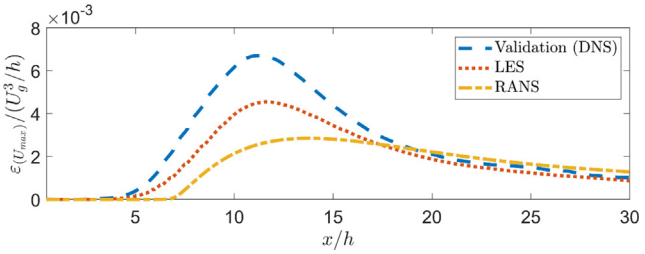

Fig. 10. Dissipation rate of TKE, ε, on the centerline of the jet, as a function of the streamwise distance, x. The validation data (DNS) is compared to the predictions using the two turbulence models under investigation (LES and RANS).

ing DSD (via a PBE approach). A more relevant comparison on how the two turbulence modelling approaches perform on an emulsification device can therefore be made by looking at the difference in terms of drop diameter predictions.

The typical aim when performing a CFD on an emulsification device is to obtain an estimate of the average effective dissipation rate of TKE, to be used in a Kolmogorov-Hinze type of equation to predict the largest drop surviving prolonged exposure to the device (i.e., maximum drop diameter obtained after repeated passages). The average dissipation rate of TKE (across a region $0 < x/h < 20$, $0.5 < y/h < 2.5$) is $\varepsilon^* = 2.4\ 10^4\ m^2/s^3$, according to the validation data. Inserted into the viscosity-modified Kolmogorov-Hinze equation, i.e. Eq. (6), this results in $D_{max} = 27.0$ μm. Table 1 compares this to the corresponding estimate using the data from the LES and RANS to model turbulence, as well as to traditional scaling-based estimates of the droplet diameter (see Eq. (7) and Eq. (8)). LES gives the most accurate predictions, both in terms of dissipation rate of TKE (-12%) and in terms of the resulting D_{max} (+4.8%) (Note that the relative error in the maximum drop diameter estimate is smaller than that of the dissipation rate of TKE, due to the sub-linear scaling of ε^* on D_{max} in Eq. (6)). RANS has a substantially lower accuracy, −38% for ε^* and +18% for D_{max}. However, RANS still offers a large improvement from traditional scale-base estimations: Eq. (8) (Innings and Trägårdh, 2007) overestimates ε^* by almost a factor of 2 and Eq. (7) (Mohr, 1987) overestimates it by a factor of 7, leading to a relative error of −31% and −57% when translated into maximum drop diameter.

3.3.3. From trajectories to PBE estimated DSDs

Most recent studies, however, are to an increasing extent moving from assessing the efficiency of emulsification devices from the characteristic dissipation rate of TKE, to using PBE models (see Section 1). A PBE evaluation has the advantage of taking into account both the distribution of turbulent stresses and that of the velocity, and is, therefore, expected to provide a better estimate of the device performance (at least if appropriate fragmentation kernels have been identified).

Fig. 10 displays the dissipation rate of TKE on the trajectory through the centerline of the jet, comparing the two CFD models with the validation data (DNS). As seen previously, both LES and RANS underestimate the maximum value of the dissipation rate of TKE. Thus, both turbulence models are expected to underestimate the amount of breakup taking place in the device. Also note that both models provide good estimate further downstream of the gap exit.

As noted in the introduction, there is yet no general consensus on which breakup frequency and fragment size distribution best describes breakup in emulsification devices. However, the fragmentation rate suggested by Luo and Svendsen (1996) is a good candidate for a first comparison, being free of empirical fitting parameters. Solving the fragmentation only PBE (Eq. (9)) across the validation data trajectory in Fig. 10, results in a Sauter mean diameter of $D_{32} = 20.7$ μm. When integrated across the trajectory, the D_{32} predictions based on the PBE are similar between LES and RANS (error of ∼ 20%, see Table 1). This can be somewhat surprising given that the LES model captures the peak dissipation rate of TKE better than the RANS model (see Fig. 10). However, RANS data overpredict dissipation rates further downstream ($x/h = 20$–30), thus prescribing a higher fragmentation rate at these positions, which compensates for the underestimation of the peak and leads to a similar value of the Sauter mean diameter.

The alternative to using a CFD model to provide profiles of the dissipation rate of TKE needed for the PBE, would be to use scaling-law estimations (Eqs. 7–8) (cf. Håkansson et al., 2009; Maindarkar et al., 2015; Raikar et al., 2010). The corresponding PBE-estimates based on Eq. (7) and Eq. (8) were calculated assuming that.

$$\varepsilon(t) = \begin{cases} \varepsilon^* & t \leq \frac{U_g}{20h} \\ 0 & elsewise \end{cases} \tag{11}$$

Results are summarized in Table 1, showing how the scale-based estimates results in substantially lower accuracy in the estimation of D_{32} compared to the RANS (−54% and −77% with Eqs. (8) and (7) respectively).

Summarizing, the LES model does typically provide a more accurate characterization of the efficiency of the device, but the RANS is not far behind and provides a substantial improvement when compared to traditional scaling models. As basis for the PBE integration, LES and the RANS perform equally well (although this is largely due to a fortunate cancellation of under- and over-prediction in different areas).

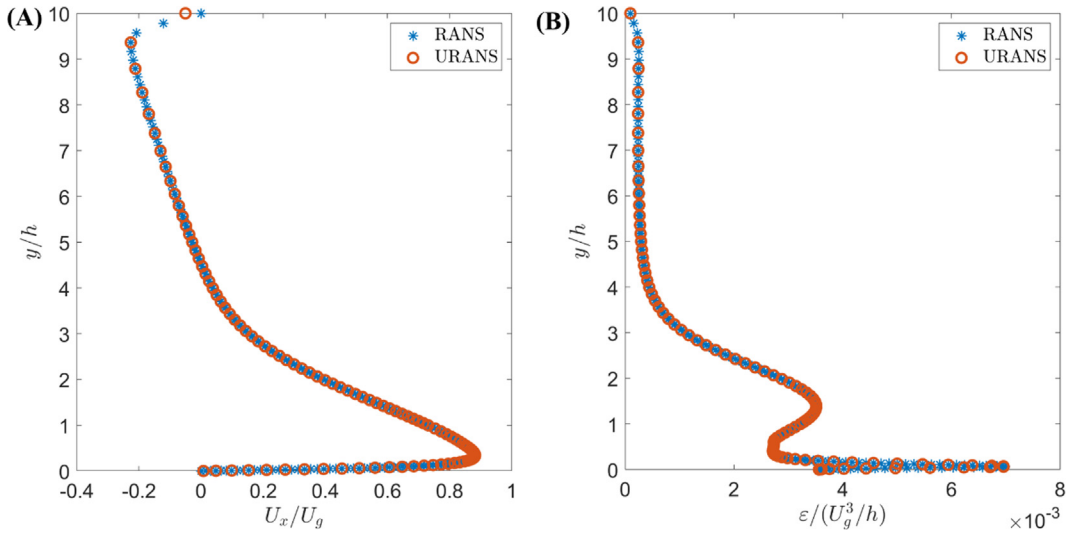

Fig. 11. Comparing (A) the average streamwise velocity, U_x, and (B) the dissipation rate of TKE, ε, as function of wallnormal distance, y, between RANS and URANS. (x/h = 16).

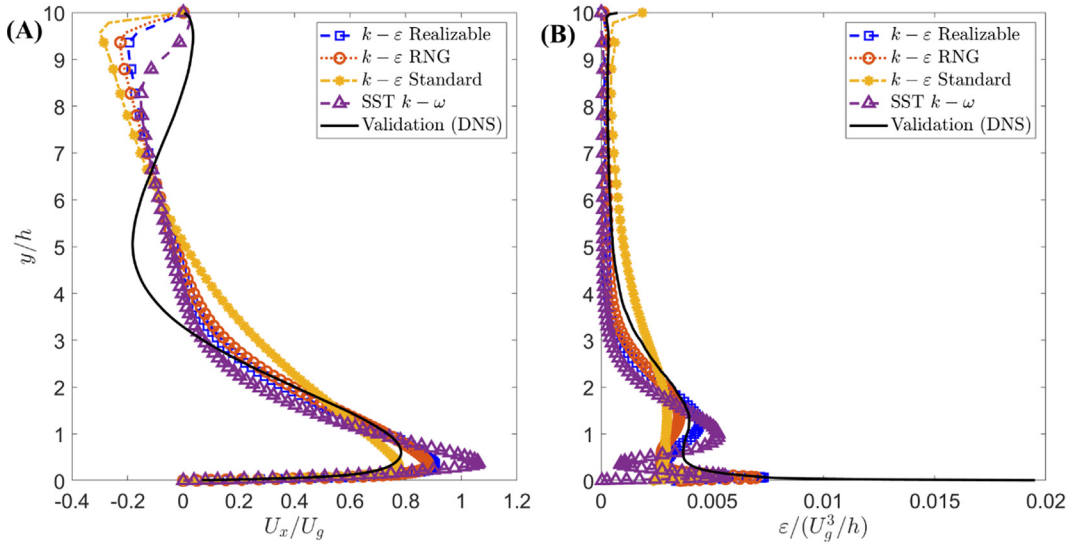

Fig. 12. Comparing (A) the average streamwise velocity, U_x, and (B) the dissipation rate of TKE, ε, as function of wallnormal distance, y, between three different two-equation RANS models: standard k – ε, RNG k – ε, realizable k – ε, and SST k – ω. (x/h = 16).

3.4. RANS model settings

The comparisons above are all based on a 2D steady RANS with an RNG k – ε turbulence model. As seen in Section 2.4, the solution is mesh independent. However, from a best practice perspective, it is interesting to understand how sensitive the accuracy of the RANS model is to model settings, especially in the light of the variations seen when considering the available CFD investigations of the HPH outlet chambers (see Section 1).

3.4.1. Transient formulation

Unsteady RANS (URANS) do sometimes perform better in predicting turbulent flows, compared to the steady RANS used in this investigation. Fig. 11 therefore includes a comparison with a URANS with the same mesh and turbulence model (RNG k – ε) as the RANS. No differences can be seen between the RANS and the URANS. Consequently, URANS does not improve the accuracy of the estimates and is, therefore, not necessary in this case.

3.4.2. Turbulence modelling

As seen from the literature review, previous studies applying two-equation RANS models to HPH valves typically used either realizable k – ε, RNG k – ε or standard k – ε. Fig. 12 compares the RANS-predicted velocity magnitudes and TKE dissipation rate at x/h = 16, for these three RANS models and the SST k – ω model, which is a conventional approach often used in industry, against the validation DNS data. As observed in the figure, standard k – ε performs poorly, which has previously been attributed to its inability to handle curved streamlines and recirculation in the outlet chamber (Håkansson et al., 2012). This inability for standard k – ε to correctly predict the details of turbulent flows is well-known and a reason for the general favor towards the improved methods. The realizable and RNG k – ε models give rise to improved estimations when compared to validation data (see Fig. 12), with differences between the two being relatively small. Comparing to the DNS shows that the RNG k – ε performs slightly better. This is seen more clearly when attempting to use the realizable k – ε RANS

Table 2
Comparison of computational time.

	Computational time per 1 ms physical time [core h]	Convergence time (physical) [ms]	Data sampling time (physical) [ms]	Total computational time (convergence + sampling) [core h]	Total computational time [relative DNS]
DNS (validation)	1 000*	2000 t_g = 94 ms	3000 t_g = 140 ms	230 000	100%
LES	200**	4000 t_g = 188 ms	3000 t_g = 140 ms	66 000	29%
RANS				64**	0.03%

$t_g = h/U_g = 47$ μs.
* Using HPC-resource, 800 cores.
** Using office workstation, 64 cores.

model to predict the Sauter mean diameter on particle trajectory (cf. Table 1). Indeed, the RNG k – ε only resulted in a relative error of 22% compared to the validation data, while the realizable k – ε leads to a relative error of 61%. Note that, regardless of the model used, there is still a difference with the validation data. Exactly which of the modelling assumptions in these models that are responsible for these differences is unknown. One suggestion offered in a previous study (Håkansson et al., 2012) is their inability to handle negative production of TKE, which leads to an overprediction of the production term.

Fig. 12 also includes a comparison to the SST k – ω model, which overpredicts both the streamwise velocity and the dissipation rate of TKE at the peak values. This limitation of SST k – ω is not general (for many other flows, this model outperforms the models of the k – ε family), but it is in-line with results from a previous validation on a similar wall-interaction confined jet (Mortensen et al., 2018).

In summary, in this setting, the RNG k – ε is the preferred choice.

3.5. Computational cost

The performance of the different approaches to predict the turbulent properties of the outlet chamber needs to be seen in the light of their computational cost. Table 2 compares the computational cost for the LES and RANS models to the computational cost of generating the validation data with DNS. Starting with the DNS, a converged flow-field requires simulating 94 ms of physical time and an additional 140 ms for data sampling (Olad et al., 2022). When running this setup at the national high performance computing (HPC) resources, Tetralith (Xeon Gold 6130, 3 10^{15} flops/s on LINPACK) and Beskow (Crey XC40, 1.810^{15} flops/s on LINPACK), on 800 cores, each 1 ms of simulation required 1000 core hours. Thus, generating DNS data for a single geometry and flow-setting requires approximately 230 000 core hours. This high computational cost further illustrates that DNS, whereas highly valuable for generating validation data and building fundamental understanding, is still unsuitable for routine investigations or in an industrial or device design setting.

The LES comes at a lower computational cost. Each ms of physical time simulated require 200 core hours on a local workstation. Convergence and sampling requires running for approximately 7000 t_g, resulting in a total LES computational cost which is 29% of the DNS's. Here it should be noted that the LES cost would be substantially lower if the case was also run at an HPC resource (as the DNS). However, Table 2 still shows that LES leads to a substantial reduction in computational cost. Nevertheless, the cost is such that LES is still relatively rare in CFD simulations of HPH valves.

The RANS is a steady state simulation and required only a total of 64 core hours. This is 0.03% of the computational time of the DNS or 0.1% of the cost of the LES, showing the considerable reduction by choosing a RANS instead of an LES.

3.6. Best practice discussion

Regardless of if investigating the overall time-averaged flow (Fig. 5), jet half-width and velocity (Fig. 7), the dissipation rate of TKE (Fig. 8) or resulting drop diameter from different correlations and models (Table 1), the high-resolution LES provides more accurate estimates. This is, in itself, expected because two-equation RANS models rely on severe modelling assumptions (Pope, 2000). It is also well-known that RANS results in a substantially lower computational cost than LES (especially when a steady 2D formulation can be used). From the perspective of the applied emulsification researcher, interested in the time-averaged velocity and dissipation of TKE field as an input to a PBE study, or for the R&D team searching for a method to screen valve designs, the interesting question is how much more accurate the LES is and how much higher the computational cost is.

These investigations show that the RANS performs relatively well, both in terms of velocity field and dissipation rate of TKE for investigators mainly interested in the flow inside the jet. However, only when not requiring high accuracy close to the inlet (where the RANS struggles due to its simplistic inlet boundary specification) or close to the outlet (where the RANS struggles to describe the outlet-vortex created by the confinement together with the outlet boundary condition). The characteristic dissipation rate of TKE is underpredicted by the RANS, leading to an overprediction the maximum drop diameter which is substantially higher for the RANS than for the LES. When applied to a PBE (Section 3.3.3), however, the difference reduces. Combined with the substantially lower computational cost of the RANS (factor of 970 compared to the LES), it could be argued that a (mesh-independent) RANS has its use in, for example, PBE investigations or valve design screening. Here it should also be kept in mind that the LES used in this study is (by design) a highly resolved LES (i.e., fulfilling the minimum 80% of resolved TKE criteria). Comparing the RANS to a LES with a lower percentage of modelled TKE, provides a stricter comparison than comparing to a VLES or hybrid-LES (which would often be the alternative to using RANS in an applied emulsification research or industrial setting, cf. Taghinia et al., 2016).

Section 3.5 also allows for a discussion on what is required of the RANS to achieve this acceptable performance. HPH valves are not planar, thus a true 2D model is an approximation; however, the axisymmetry of the devices allows for a axi-symmetrical 2D formulation. Industrially relevant HPH valves will typically be fed with an inlet velocity that oscillates with a small amplitude (due to the 3–5 piston pumps used in creating the high static inlet pressure), which has a minor effect on hydrodynamics for production

scale systems (Håkansson, 2018), suggesting that a steady RANS, axisymmetrical 2D formulation, enhanced wall treatment and RNG k – ε would be a suitable methodology for modelling HPH outlet chambers. Importantly, the solution must be showed to be mesh independent (cf. Fig. 11).

Examining the surprisingly good performance of the RANS (given its theoretical limitations), one must still keep in mind that the LES model provides more accurate estimations (as clearly showed by the results of this contribution), regardless of the parameter under investigation. Moreover, an LES will provide many pieces of information that could be of interest from an industrial perspective and that is inaccessible from a RANS analysis. A RANS is, for example, unable to make any predictions about the stochastic time variations in the instantaneous stresses (i.e., in the instantaneous dissipation rate of TKE and probability distribution thereof), which plays an important role in influential drop breakup theories (Baldyga and Podgórska, 1998) as well as in recent suggestions on extending CFD-PBE methodology (Aiyer et al., 2019). An LES model, but not a RANS model, can also be used to estimate the power spectra, and, consequently, any non-ideal behaviour in these. This is another limitation of the RANS methodology with potential implications for applied emulsification research since such anisotropy-induced peaks in the spectra have recently been suggested as important to correctly describe fragmentation rates in Sonolators (Bagkeris et al., 2020). A third (and final) advantage of LES is the possibility for turbulent eddy visualizations. This is another tool that has proven useful in characterizing emulsification systems (Andersson and Helmi, 2014).

4. Conclusions

The overall aim of this study was to conclude on how well LES and RANS CFD performs in predicting the flow properties relevant for characterizing the efficiency of a confined turbulent wall jet similar to that in a high-pressure homogenizer valve, using DNS data for validation. Moreover, we have used these insights to comment on best practices for CFD modelling strategies. Returning to the specific research questions in the introduction, it can be concluded that:

- Both the LES and the RANS are able to reproduce the general outline of the time-averaged velocity field in the outlet chamber; more specifically, both models are able to predict jet velocities and jet half-width, especially when considering the region where breakup is expected to occur. The LES provides a more accurate estimate (especially of the effect of the macroscopic vortices), but the difference in terms of jet half-width and velocity is relatively small.
- The LES does provide a substantial improvement over the RANS in terms of predictions of the global maximum dissipation rate of TKE as well as in terms of the local profiles thereof, especially in the thin region closest to the lower wall. However, in the of the jet, at the positions where drop breakup is expected to take place, the differences are relatively small. Here, please note that the investigations in this contribution are made with a relatively highly resolved LES. Differences between RANS and a VLES or hybrid-LES (as in previous studies modelling emulsification devices) are expected to be smaller.
- When using the LES and RANS models to estimate a characteristic dissipation rate of TKE for the device, the LES performs better than the RANS. Translated into predicted maximum drop diameter surviving prolonged exposure to the device, the LES overpredicts D_{max} by 4.8% (compared to the validation data) whereas the RANS overpredicts D_{max} by 18%. The RANS does, however, result in a substantial improvement compared to the current alternative (i.e., traditional empirical equations based on scaling arguments), which gives an underprediction of 31–57% depending on which of the models suggested in literature is used. When instead compared in terms of what average drop size the LES and RANS data would predict in a PBE setting, LES and RANS result in approximately the same relative error (∼20%), which, again, is substantially better than the results of traditional scale-based estimations (resulting in a relative error of 54–77%).
- A comparison of different settings of the RANS model shows that a steady 2D formulation is a preferred choice (cost, but not accuracy, increases by using a 3D and/or URANS formulation). Moreover, RNG k – ε provides the highest accuracy of the investigated two-equation RANS models.

Overall, this study shows that RANS simulations (despite their substantial theoretical limitations compared to more advanced approaches such as LES), remain a relevant supplementary tool for estimating velocity fields and obtaining a fairly accurate dissipation rate of TKE also given their substantially lower computational cost.

CRediT authorship contribution statement

Peyman Olad: Conceptualization, Methodology, Software, Data curation, Validation, Formal analysis, Investigation, Visualization, Writing – original draft, Writing – review & editing. **Marco Crialesi Esposito:** Resources, Software, Writing – review & editing. **Luca Brandt:** Supervision, Resources, Writing – review & editing. **Fredrik Innings:** Conceptualization, Supervision, Writing – review & editing, Funding acquisition. **Andreas Hakansson:** Conceptualization, Methodology, Resources, Writing – original draft, Writing – review & editing, Project administration, Funding acquisition.

Declaration of Competing Interest

The authors declare that they have no known competing financial interests or personal relationships that could have appeared to influence the work reported in this paper.

Acknowledgments

Dr. Fredrik Carlsson and Prof. Johan Revstedt are greatfully acknowledged for valuable discussion and insights, helpful for setting up the LES and RANS models. This study was financed by the Swedish Research council (VR), grant number 2018-03820 and Tetra Pak Processing Systems AB. The computations and data handling (DNS) were enabled by resources provided by the Swedish National Infrastructure for Computing (SNIC) at PDC and NSC, partially funded by the Swedish Research Council through grant agreement no. 2018-05973. Computations (LES) were enabled by resources provided by Tetra Pak.

Appendix A. Supplementary material

Supplementary data to this article can be found online at https://doi.org/10.1016/j.ces.2022.117748.

References

Aiyer, A.K., Yang, D., Chamecki, M., Meneveau, C., 2019. A population balance model for large eddy simulation of polydisperse droplet evolution. J. Fluid Mech. 878, 700–739. https://doi.org/10.1017/jfm.2019.649.

Andersson, R., Helmi, A., 2014. Computational fluid dynamics simulation of fluid particle fragmentation in turbulent flows. Appl. Math. Model. 38 (17-18), 4186–4196.

ANSYS. (2019). Fluent. Canonsburg, PA: ANSYS. Retrieved from http://www.ansys.com/products/fluids/ansys-fluent.

Arai, K., Konno, M., Matunaga, Y., Saito, S., 1977. Effect of dispersed-phase viscosity on the maximum stable drop size for breakup in turbulent flow. J. Chem. Eng. Jpn. 10 (4), 325–330. https://doi.org/10.1252/jcej.10.325.

Bagkeris, I., Michael, V., Prosser, R., Kowalski, A., 2020. Large–eddy simulation in a Sonolator high–pressure homogeniser. Chem. Eng. Sci. 215, 115441. https://doi.org/10.1016/j.ces.2019.115441.

Baldyga, J., Podgórska, W., 1998. Drop break-up in intermittent turbulence: Maximum stable and transient sizes of drops. Can. J. Chem. Eng. 76 (3), 456–470.

Becker, P.J., Puel, F., Dubbelboer, A., Janssen, J., Sheibat-Othman, N., 2014. Coupled population balance–CFD simulation of droplet breakup in a high pressure homogenizer. Comput. Chem. Eng. 68, 140–150. https://doi.org/10.1016/j.compchemeng.2014.05.014.

Billson, M., Eriksson, L.-E., Davidson, L. (2003). Jet Noise Prediction Using Stochastic Turbulence Modeling. South Carolina: American Institute of Aeronautics and Astronautics. 10.2514/6.2003-3282.

Bisten, A., Schuchmann, H., 2016. Optical measuring methods for the investigation of high-pressure homogenisation. Processes 4 (4), 41. https://doi.org/10.3390/pr4040041.

Calabrese, R.V., Chang, T.P., Dang, P.T., 1986. Drop breakup in turbulent stirred-tank contactors. Part I: Effect of dispersed-phase viscosity. AIChE J. 32 (4), 657–666. https://doi.org/10.1002/aic.690320416.

Casoli, P., Vacca, A., Berta, G.L., 2010. A numerical procedure for predicting the performance of high pressure homogenizing valves. Simul. Model. Pract. Theory 18 (2), 125–138. https://doi.org/10.1016/j.simpat.2009.09.014.

Davidson, L., Billson, M., 2006. Hybrid LES-RANS using synthesized turbulent fluctuations for forcing in the interface region. Int. J. Heat Fluid Flow 27 (6), 1028–1042. https://doi.org/10.1016/j.ijheatfluidflow.2006.02.025.

Davies, J., 1985. Drop sizes of emulsions related to turbulent energy dissipation rates. Chem. Eng. Sci. 40 (5), 839–842. https://doi.org/10.1016/0009-2509(85)85036-3.

Dubbelboer, A., Janssen, J., Hoogland, H., Mudaliar, A., Maindarkar, S., Zondervan, E., Meuldijk, J., 2014. Population balances combined with Computational Fluid Dynamics: A modeling approach for dispersive mixing in a high pressure homogenizer. Chem. Eng. Sci. 117, 376–388. https://doi.org/10.1016/j.ces.2014.06.047.

Rosti, M.E., De Vita, F., Brandt, L., 2019. Numerical simulations of emulsions in shear flows. Acta Mech 230 (2), 667–682.

Floury, J., Bellettre, J., Legrand, J., Desrumaux, A., 2004. Analysis of a new type of high pressure homogeniser. A study of the flow pattern. Chem. Eng. Sci. 59 (4), 843–853.

Germano, M., Piomelli, U., Moin, P., Cabot, W.H., 1991. A dynamic subgrid-scale eddy viscosity model. Phys. Fluids A 3 (7), 1760–1765. https://doi.org/10.1063/1.857955.

Gerodimos, G., So, R.M.C., 1997. Near-Wall Modeling of Plane Turbulent Wall Jets. J. Fluids Eng. 119 (2), 304–313. https://doi.org/10.1115/1.2819135.

Guan, X., Yang, N., Nigam, K.D., 2020. Prediction of droplet size distribution for high pressure homogenizers with heterogeneous turbulent dissipation rate. Ind. Eng. Chem. Res. 59 (9), 4020–4032. https://doi.org/10.1021/acs.iecr.9b04615.

Håkansson, A., 2018. Flow pulsation plays an important role for high-pressure homogenization in laboratory-scale. Chem. Eng. Res. Des. 138, 472–481. https://doi.org/10.1016/j.cherd.2018.09.015.

Håkansson, A., Fuchs, L., Innings, F., Revstedt, J., Trägårdh, C., Bergenståhl, B., 2011. High resolution experimental measurement of turbulent flow field in a high pressure homogenizer model and its implications on turbulent drop fragmentation. Chem. Eng. Sci. 66 (8), 1790–1801. https://doi.org/10.1016/j.ces.2011.01.026.

Håkansson, A., Fuchs, L., Innings, F., Revstedt, J., Trägårdh, C., Bergenståhl, B., 2012. Experimental validation of k–ε RANS-CFD on a high-pressure homogenizer valve. Chem. Eng. Sci. 71, 264–273. https://doi.org/10.1016/j.ces.2011.12.039.

Håkansson, A., Innings, F., Trägårdh, C., Bergenståhl, B., 2013. A high-pressure homogenization emulsification model—Improved emulsifier transport and hydrodynamic coupling. Chem. Eng. Sci. 91, 44–53. https://doi.org/10.1016/j.ces.2013.01.011.

Håkansson, A., Trägårdh, C., Bergenståhl, B., 2009. Studying the effects of adsorption, recoalescence and fragmentation in a high pressure homogenizer using a dynamic simulation model. Food Hydrocolloids 23 (4), 1177–1183. https://doi.org/10.1016/j.foodhyd.2008.10.003.

Hinze, J.O., 1955. Fundamentals of the hydrodynamic mechanism of splitting in dispersion processes. AIChE J. 1 (3), 289–295. https://doi.org/10.1002/aic.690010303.

Innings, F., Trägårdh, C., 2005. 08). Visualization of the Drop Deformation and Break-Up Process in a High Pressure Homogenizer. Chem. Eng. Technol. 28 (8), 882–891. https://doi.org/10.1002/ceat.200500080.

Innings, F., Trägårdh, C., 2007. Analysis of the flow field in a high-pressure homogenizer. Exp. Therm Fluid Sci. 32 (2), 345–354. https://doi.org/10.1016/j.expthermflusci.2007.04.007.

Innings, F., Fuchs, L., Trägårdh, C., 2011. Theoretical and experimental analyses of drop deformation and break-up in a scale model of a high-pressure homogenizer. J. Food Eng. 103 (1), 21–28. https://doi.org/10.1016/j.jfoodeng.2010.09.016.

Jiang, B., Shi, Y., Lin, G., Kong, D., Du, J., 2019. Nanoemulsion prepared by homogenizer: The CFD model research. J. Food Eng. 241, 105–115. https://doi.org/10.1016/j.jfoodeng.2018.08.014.

Kader, B., 1981. Temperature and concentration profiles in fully turbulent boundary layers. Int. J. Heat Mass Transf. 24 (9), 1541–1544. https://doi.org/10.1016/0017-9310(81)90220-9.

Kelemen, K., Gepperth, S., Koch, R., Bauer, H.J., Schuchmann, H.P., 2015. On the visualization of droplet deformation and breakup during high-pressure homogenization. Microfluid. Nanofluid. 19 (5), 1139–1158. https://doi.org/10.1007/s10404-015-1631-z.

Kelly, W.J., Muske, K.R., 2005. Optimal operation of high-pressure homogenization for intracellular product recovery. Bioprocess Biosyst Eng 27 (1), 25–37.

Kleinig, A.R., Middelberg, A.P., 1996. The correlation of cell disruption with homogenizer valve pressure gradient determined by computational fluid dynamics. Chem. Eng. Sci. 51 (23), 5103–5110. https://doi.org/10.1016/S0009-2509(96)00354-5.

Kleinig, A.R., Middelberg, A.P.J., 1997. Numerical and experimental study of a homogenizer impinging jet. AIChE J. 43 (4), 1100–1107. https://doi.org/10.1002/aic.690430423.

Köhler, K., Aguilar, F.A., Schubert, H., Hensel, A., Schubert, K., Schuchmann, H.P., 2008. Design of a Microstructured System for the Homogenization of Dairy Products at High Fat Content Part II: Influence of Process Parameters. Chem. Eng. Technol. 31 (12), 1863–1868.

Kolmogorov, A., 1949. On the breakage of drops in a turbulent flow. Dokl. Akad. Navk. SSSR 66, 825–828.

Kumar, S., Ramkrishna, D., 1996. On the solution of population balance equations by discretization—I. A fixed pivot technique. Chem. Eng. Sci. 51 (8), 1311–1332. https://doi.org/10.1016/0009-2509(96)88489-2.

Launder, B.E., Spalding, D.B. (1972). Lectures in mathematical models of turbulence. London, New York: Academic Press. Retrieved from https://nla.gov.au/nla.cat-vn1970799.

Liao, Y., Lucas, D., 2009. A literature review of theoretical models for drop and bubble breakup in turbulent dispersions. Chem. Eng. Sci. 64 (15), 3389–3406. https://doi.org/10.1016/j.ces.2009.04.026.

Lilly, D.K. (1992). A proposed modification of the Germano subgrid-scale closure method. 4(3), 633–635. https://doi.org/10.1063/1.858280

Luo, H., Svendsen, H.F., 1996. Theoretical model for drop and bubble breakup in turbulent dispersions. AIChE J. 42 (5), 1225–1233. https://doi.org/10.1002/aic.690420505.

Maindarkar, S.N., Hoogland, H., Henson, M.A., 2015. Predicting the combined effects of oil and surfactant concentrations on the drop size distributions of homogenized emulsions. Colloids Surf., A 467, 18–30. https://doi.org/10.1016/j.colsurfa.2014.11.032.

Mathey, F., Cokljat, D., Bertoglio, J.-P., Sergent, E., 2006. 01). Specification of LES inlet boundary condition using vortex method. Progr. Comput. Fluid Dyn. 6, 58–67. https://doi.org/10.1504/PCFD.2006.009483.

Menter, F. R. (1994). Two-equation eddy-viscosity turbulence models for engineering applications. 32(8), 1598-1605. https://doi.org/10.2514/3.12149

Miller, J., Rogowski, M., Kelly, W., 2002. Using a CFD Model To Understand the Fluid Dynamics Promoting E. coli Breakage in a High-Pressure Homogenizer. Biotechnol. Prog. 18 (5), 1060–1067.

Mohr, K.-H., 1987. High-pressure homogenization. Part I. Liquid-liquid dispersion in turbulence fields of high energy density. J. Food Eng. 6 (3), 177–186. https://doi.org/10.1016/0260-8774(87)90023-9.

Mortensen, H.H., Arlov, D., Innings, F., Håkansson, A., 2018. A validation of commonly used CFD methods applied to rotor stator mixers using PIV measurements of fluid velocity and turbulence. Chem. Eng. Sci. 177, 340–353. https://doi.org/10.1016/j.ces.2017.11.037.

Mutsch, B., Preiss, F.J., Dagenbach, T., Karbstein, H.P., Kähler, C.J., 2021. Scaling of Droplet Breakup in High-Pressure Homogenizer Orifices. Part II: Visualization of the Turbulent Droplet Breakup. ChemEngineering 5 (2). https://doi.org/10.3390/chemengineering5020031.

Olad, P., Crialesi, M., Brandt, L., Innings, F., Håkansson, A., 2022. A DNS investigation of the one-phase flow in a simplified emulsification device. J. Fluids Eng. 144 (8). https://doi.org/10.1115/1.4053896.

Orlanski, I., 1976. A simple boundary condition for unbounded hyperbolic flows. J. Comput. Phys. 21 (3), 251–269. https://doi.org/10.1016/0021-9991(76)90023-1.

Pang, H., Ngaile, G., 2021. Modeling of a valve-type low-pressure homogenizer for oil-in-water emulsions. Chem. Eng. Process. – Process Intensificat. 160, 108249. https://doi.org/10.1016/j.cep.2020.108249.

Picano, F., Breugem, W.-P., Brandt, L., 2015. Turbulent channel flow of dense suspensions of neutrally buoyant spheres. J. Fluid Mech. 764, 463–487. https://doi.org/10.1017/jfm.2014.704.

Pope, S. (2000). Turbulent flows . Cambridge, UK: Cambridge University Press.

Raikar, N.B., Bhatia, S.R., Malone, M.F., McClements, D.J., Almeida-Rivera, C., Bongers, P., Henson, M.A., 2010. Prediction of emulsion drop size distributions with population balance equation models of multiple drop breakage. Colloids Surf., A 361 (1), 96–108. https://doi.org/10.1016/j.colsurfa.2010.03.020.

Ramkrishna, D. (2000). Population balances–Theory and applications to particulate systems in engineering. San Diego: Academic Press.

Rosti, M.E., Brandt, L., 2017. Numerical simulation of turbulent channel flow over a viscous hyper-elastic wall. J. Fluid Mech. 830, 708–735. https://doi.org/10.1017/jfm.2017.617.

Saarenrinne, P., Piirto, M., 2000. Turbulent kinetic energy dissipation rate estimation from PIV velocity vector fields. Exp. Fluids 29 (1), 5300–5307. https://doi.org/10.1007/s003480070032.

Shih, T.-H., Liou, W.W., Shabbir, A., Yang, Z., Zhu, J., 1995. A new k-ϵ eddy viscosity model for high reynolds number turbulent flows. Comput. Fluids 24 (3), 227–238. https://doi.org/10.1016/0045-7930(94)00032-T.

Solsvik, J., Tangen, S., Jakobsen, H.A., 2013. On the constitutive equations for fluid particle breakage. Rev. Chem. Eng. 29 (5), 241–356. https://doi.org/10.1515/revce-2013-0009.

Steiner, H., Teppner, R., Brenn, G., Vankova, N., Tcholakova, S., Denkov, N., 2006. Numerical simulation and experimental study of emulsification in a narrow-gap homogenizer. Chem. Eng. Sci. 61 (17), 5841–5855. https://doi.org/10.1016/j.ces.2006.04.016.

Stevenson, M.J., Chen, X.D., 1997. Visualization of the flow patterns in a high-pressure homogenizing valve using a CFD package. J. Food Eng. 33 (1), 151–165. https://doi.org/10.1016/S0260-8774(97)00046-0.

Taghinia, J., Rahman, M., Tse, K., Siikonen, T., 2016. CFD modeling of homogenizer valve: A comparative study. Chem. Eng. Res. Des. 106, 327–336. https://doi.org/10.1016/j.cherd.2015.12.014.

Tanaka, T., Eaton, J.K., 2007. A correction method for measuring turbulence kinetic energy dissipation rate by PIV. Exp. Fluids 42 (6), 893–902. https://doi.org/10.1007/s00348-007-0298-y.

Vankova, N., Tcholakova, S., Denkov, N.D., Ivanov, I.B., Vulchev, V.D., Danner, T., 2007. Emulsification in turbulent flow: 1. Mean and maximum drop diameters in inertial and viscous regimes. J. Colloid Interface Sci. 312 (2), 363–380. https://doi.org/10.1016/j.jcis.2007.03.059.

Wang, G., Yang, F., Wu, K.e., Ma, Y., Peng, C., Liu, T., Wang, L.-P., 2021. Estimation of the dissipation rate of turbulent kinetic energy: A review. Chem. Eng. Sci. 229, 116133. https://doi.org/10.1016/j.ces.2020.116133.

Wolfshtein, M., 1969. The velocity and temperature distribution in one-dimensional flow with turbulence augmentation and pressure gradient. Int. J. Heat Mass Transf. 12 (3), 301–318. https://doi.org/10.1016/0017-9310(69)90012-X.

Yakhot, V., Orszag, S.A., 1986. Renormalization group analysis of turbulence. I. Basic theory. J. Sci. Comput. 1 (1), 3–51. https://doi.org/10.1007/BF01061452.